Hindawi
Journal of Spectroscopy
Volume 2022, Article ID 2281477, 6 pages
https://doi.org/10.1155/2022/2281477

Research Article

A Raman Spectroscopic Study of Calcium Silicate Hydrate (CSH) in the Cement Matrix with CNTs and Oxide Additives

Muhammad Azeem[1] **and Muhammad Azhar Saleem**[2]

[1]*Department of Applied Physics and Astronomy, University of Sharjah, University City, Sharjah 27272, UAE*
[2]*Department of Civil Engineering, Ajman University, Ajman, UAE*

Correspondence should be addressed to Muhammad Azeem; mazeem@sharjah.ac.ae

Received 15 February 2022; Revised 26 March 2022; Accepted 1 April 2022; Published 26 April 2022

Academic Editor: Petre Makreski

The calcium silicate hydrate (CSH) concentration in the cement paste mixed with different types of carbon nanotubes (CNTs) and oxide additives is compared by using Raman spectroscopy. The pristine, hydroxyl and carboxyl functionalized CNTs are used in this work. The oxide additives are zinc oxide (ZnO), gadolinium oxide (Gd_2O_3), and silicon oxide (SiO_2). A laser wavelength of 785 nm was used to collect the Raman spectra. It was observed that the concentration of calcium silicate hydrate (CSH) is unaffected in CNTs-OPC matrices regardless of the type and weight percentage of the CNTs. The oxides, as expected, show significant effects on the concentration of the CSH in the matrices. An increase in the CSH concentration is observed in the ZnO and Gd_2O_3 matrices with cement. For the SiO_2 cement paste matrix, however, the CSH concentration appears to be decreased. This study shows CSH concentration can be controlled by using oxide additives whereas CNTs do not react chemically with the cement composites.

1. Introduction

Hydration in ordinary Portland cement is a complex chemical process that involves silicate material phases. The hydrated silicates provide mechanical strength to the concrete structure. Calcium silicate hydrate (CSH) is a major hydration compound that gives strength to a binder. The formation and the composition of CSH depends upon variable hydration conditions, such as the hydration rate [1, 2], the density and the types of pure or impure silicates, sulphates and aluminates or the foreign elements and the compounds [3, 4], water to cement ratio [5, 6], and the calcium to silicon ratio [7]. However, it is not known whether its concentration can be controlled or not. This is, partly, due to a poor understanding of reaction kinetics in the cement paste matrix with additives. The CSH has an amorphous structure, therefore, its concentration cannot be studied by using X-ray diffraction techniques. Raman spectroscopy, however, can be employed to identify the phases of CSH. It is expected that certain additives can increase or decrease CSH concentration in a cement paste matrix. In this study, an attempt is made to understand the reaction kinetics of the formation of CSH in presence of carbon nanotubes (CNTs) as well as oxide additives such as ZnO, Gd_2O_3, and SiO_2. Carbon nanotubes appear to affect the physical properties [8–10], and mechanical strength [11] of the cement paste matrix. While graphene oxide [12–14] and CNTs [15] have got a fair amount of attention as an additive to cement paste by various researchers, the metal oxides have been ignored. The oxides of choice in this work are insulators so they would not affect the electrical conductivity of the matrices. However, due to their propensity to react with the compounds present in the cement, it is expected that they form new hydrated compounds which would affect their physical properties.

There is an extraordinarily wide choice of additives to make a cement paste matrix. A combination of micro-and nanomaterials is found to affect the mechanical [16, 17], physical [18, 19], and durability properties of the cement paste [20–22]. The additives fill the voids in the matrix to

make it dense and inhomogeneous, however, a change in electronic and crystal structures of the matrix is also reported [23]. Barium enhances the hydration activity and deforms the crystal structure of the silicates [24]. Nanolimestone is found to affect the calcium to silicon ratio [2, 6] in a matrix, which leads to a modified crystal structure of the composites. The carbon-based nanostructures [9, 11, 15, 25, 26] exhibit an improved elastic modulus and flexural toughness [27]. Interestingly, the compressive strengths [11] and the flowability [10] decrease when CNTs' weight percentage increases in a matrix.

The abovementioned discussion clearly shows that the additives do affect the physical and mechanical properties of a matrix. However, no report mentions how the additives affect the CSH, the main compound of a binder. This report is concerned with the concentration of CSH in the matrices with certain additives researchsquare.com [28].

2. Materials and Methods

The ordinary Portland cement (OPC) of Type I was used for the preparation of cement paste matrices. The water-to-cement ratio was kept at 0.4 for each specimen. The carbon nanotubes (CNTs), on average, were around 10–30 μm long with an average diameter of approximately 30–50 nm. Three types of carbon nanotubes, pristine, hydroxyl functionalized (-OH), and carboxyl (-COOH) functionalized, were used to prepare specimens for this report. All oxides (ZnO, SiO_2, and Gd_2O_3) were in a 99.9% purity state. The additives were mixed in water first, by using a bench mixer. The mixer was running for two minutes to ensure that the additives are nearly uniformly mixed in the water. Cement powder was gradually added to the mixture while the mixer was running, and the mixing was carried out for 15 minutes. The proportion of each type of additive was 0.2 wt% and 0.4 wt% of the OPC. The matrices were then poured into the steel molds of size 50 mm cube and a table-type external vibrator was used for the compaction. Specimens were demolded after 1 day and then dipped in the water for four weeks for curing.

The experimental Raman spectra were obtained by using Renishaw inVia confocal Raman microscope. Ten spectra were collected from different sites of each sample, and the spectra average was calculated. Each spectrum was recorded by using a laser of wavelength 785 nm. The duration for spectrum collection was 10 seconds and the laser spot size was 50 μm. The laser power was 1% (14 mW). The use of the light source of wavelength 785 nm gives a balance between the fluorescence effects and the appropriate intensity of the Raman peaks in the sample. The fingerprint region for finding signature peaks of the hydration products is between 100 cm^{-1} and 1400 cm^{-1}. Whereas for the CNT-cement paste matrices, the spectra were collected in the energy range of 200 cm^{-1}—3000 cm^{-1}. The spectra were collected in the intervals of 500 cm^{-1} wavelengths. The spectra were then combined to obtain the full spectrum. Each sample was labeled for identification. The samples with the pristine carbon nanotubes were labeled as P-2% and P-4% indicating that the concentrations of the CNTs is 0.2 wt% and 0.4 wt%,

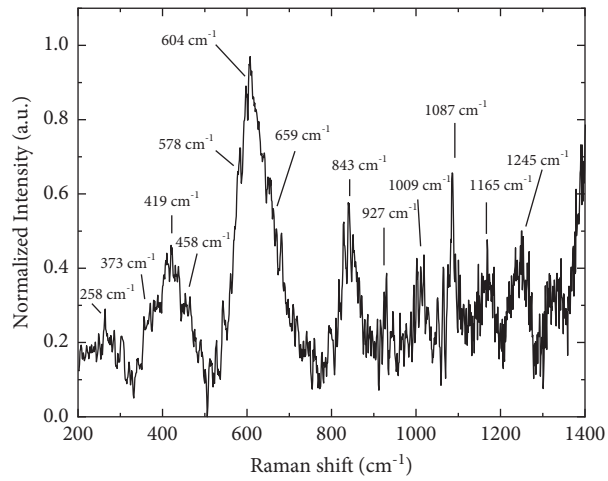

Figure 1: Experimental Raman spectrum ordinary Portland cement. The positions of the vibrational bands are indicated.

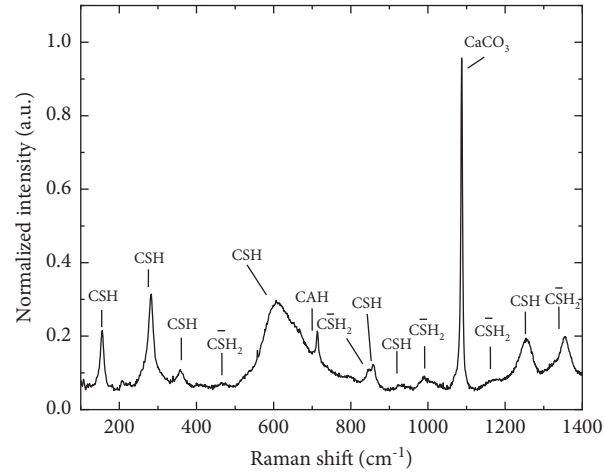

Figure 2: Experimentally obtained spectrum from a control sample of cement paste. The vibrational mode contributed by different phases present in the paste is labeled.

respectively. Other samples were labeled accordingly. All the samples used in this study are about 12 months old and the spectra were collected from the fractured surfaces.

3. Results and Discussion

3.1. Raman Spectra of Ordinary Portland Cement and the Cement Paste. Figure 1: shows the Raman spectrum for the cement powder. The values for each vibrational band are also indicated.

The Raman bands by the alite are at 373 cm^{-1}, 419 cm^{-1}, 458 cm^{-1}, 578 cm^{-1}, 604 cm^{-1}, 843 cm^{-1} and 1009 cm^{-1} [25]. The belite bands are identified as 659 cm^{-1} and 927 cm^{-1}. A peak at 258 cm^{-1} is the net effect of both the molecules, alite and the belite. The signature carbonate ($CaCO_3$) peak is at 1087 cm^{-1}. The sulphate ($CaSO_4$) and potassium sulphate (K_2SO_4) vibrational band signals are at 1165 $cm^{-1}$and 1245 cm^{-1}, respectively [25].

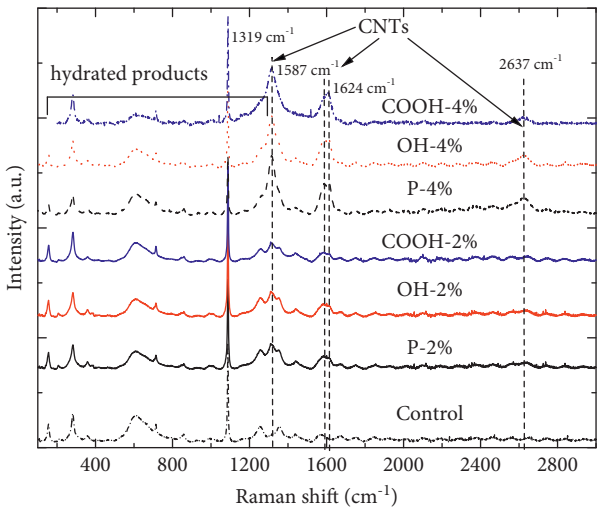

FIGURE 3: Raman spectra from the CNT-cement paste matrix. Contributions of the CNTs vibrational modes are above 1200 cm^{-1}. Raman spectra from ZnO, Gd_2O_3, and SiO_2 matrices with cement.

Figure 2 shows a spectrum obtained from a control sample of the cement paste. The band stretching between the silicon and the oxygen atoms of the alite hydrate and the $CaH_2O_5Si^{-2}$ causes the vibrational modes to occur at 292 cm^{-1} and 368 cm^{-1}. The band contributed by calcium sulphate dihydrate are at 466 cm^{-1}, 844 cm^{-1}, 997 cm^{-1}, 1164 cm^{-1} and 1355 cm^{-1}. The calcium aluminum hydride (Al_2CaH_8) phase is identified at about 713 cm^{-1}. A CSH band at the 1255 cm^{-1} is due to CaH_2O_4Si whereas all other CSH bands are contributed by $CaH_2O_5Si^{-2}$ [25]. It is, therefore, concluded that the hydrated cement paste is composed of calcium silicate hydrate (CSH) with a chemical formula $CaH_2O_5Si^{-2}$. As opposed to other CSH configurations, such as CaH_2O_4Si and $Ca_2H_2O_5Si$ where the formal charge is 0, this molecular composition has a formal charge of—2 indicative of a reactive substance.

3.2. Raman Spectra of CNT-Cement Paste Matrix. Raman spectra shown in Figure 3 is collected from the cement paste matrices with 0.2 wt% and 0.4 wt% of the pristine CNTs (P-2% and P-4%), CNTs-OH (OH-2% and OH-4%) and the CNTs-COOH (COOH-2% and COOH-4%) in the range 200 cm^{-1} to 3000 cm^{-1}. The first half of the frequency range, from 200 cm^{-1} to 1400 cm^{-1} contains signals from the hydrated products. The spectra are practically indistinguishable for different concentrations of CNTs. Also, compared to Figure 1, the spectrum of the cement paste, there are no discernible differences. This is a clear evidence that the CNTs do not form any new compounds in the matrix and do not participate in the hydration reaction. One stark feature shared by all the spectra is the splitting of the *G* band at 1587 cm^{-1} and 1624 cm^{-1}. This occurs due to the shear force applied during the mixing of the cement paste [29] and therefore some of the CNTs are graphitized. The CNTs act as nucleation sites for the hydrated crystals to grow and apply tensile stress on the CNT surface causing the *D* and the *D* overtone bands to shift to the lower frequencies, at 1319 cm^{-1} and 2637 cm^{-1}, respectively. An enhanced electrostatic interaction is caused between the cement paste composites, with the $CaH_2O_5Si^{-2}$ as a major phase. The structurally defected CNTs result in the charge imbalance at the surface of a CNT and thus strengthen the electrostatic interaction further. Another noticeable feature is that the *D* and *D* overtone bands are more intense in the specimens with higher concentrations of CNTs (P-4%, OH-4%, and COOH-4%). A high I_D/I_G ratio (>1) in these specimens indicates a greater degree of graphitization and the structural defects in the CNTs due to the mixing process and affecting the strength of the concrete [11].

The well known spectra from the SiO_2 and ZnO is shown in Figure 4. The interpretations of the spectra can be found the standard text books of Raman spectroscopy [30].

The spectra of the oxide additives with the cement paste, Figure 5, are profoundly different from the ones discussed. A strong vibrational mode of CSH is visible at 154 cm^{-1} for ZnO and Gd_2O_3, but it is not very clear for SiO_2. This feature is shared with the spectrum from the control samples as well. A weak band is present at 207 cm^{-1} in ZnO-cement paste and in Gd_2O_3-cement paste at 211 cm^{-1} but is completely absent in the control and SiO_2 cement mixtures. These features are related to the hydration of ZnO and Gd_2O_3 as will be discussed later. A strong CSH vibrational mode is visible at 281 cm^{-1} in the ZnO-cement paste, which is also shared by the control sample but is weaker in Gd_2O_3 and SiO_2 at about the same position. A CSH vibrational band at 357 cm^{-1} is shared the ZnO, SiO_2, Gd_2O_3 matrices, though much stronger in the Gd_2O_3- matrix. A Raman band by the calcium sulphate dihydrate (CaH_4O_6S) is rather weak in the control specimen, observed at 464 cm^{-1}, and is shared with the ZnO and Gd_2O_3 cement paste matrices but not with the SiO_2 cement paste. A broad and strong CSH vibrational band at 605 cm^{-1} is a common feature for all the matrices. However, it is significantly stronger in the SiO_2 and Gd_2O_3 matrices when compared with the control and CNT cement paste matrices. Calcium aluminum hydride (Al_2CaH_8) Raman band is at around 711 cm^{-1} in the control and ZnO cement paste specimens but is not shared with the SiO_2 and Gd_2O_3 matrices. Moreover, a double peak in the control, at 844 cm^{-1} and 856 cm^{-1}, supposedly the contributions from the CH_2 and CSH respectively, is replaced by a single and a broad band at around 846 cm^{-1}. A weak CSH vibrational band at 926 cm^{-1} is also shared by all the spectra. A calcium sulphate dihydrate band at about 986 cm^{-1} is relatively weak in the control and ZnO matrices, but is strong in the SiO_2 and Gd_2O_3 matrices. A strong calcium carbonate peak in control and ZnO cement paste specimens appear to be less strong in the SiO_2 and Gd_2O_3 matrices. A weak CH_2 band in control at 1168 cm^{-1} has become slightly more prominent. Finally, a very clear CSH band at 1254 cm^{-1} of the control specimen now appear to be weak in the samples with the oxide additives.

A similar trend is observed in the specimens with 0.4 wt % of the same impurities with very little differences. Strong and narrow CSH vibrational bands at 154 cm^{-1}, 282 cm^{-1} along with a clear calcium carbonate peak at around 1080 cm^{-1} are observed in 0.4 wt% SiO_2-cement paste matrix

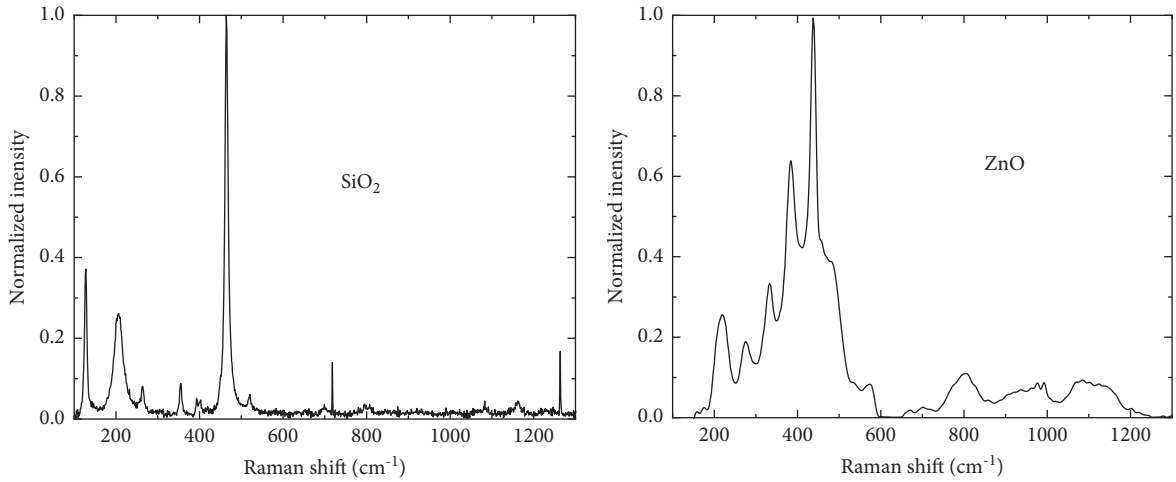

Figure 4: Raman spectra SiO_2 and ZnO.

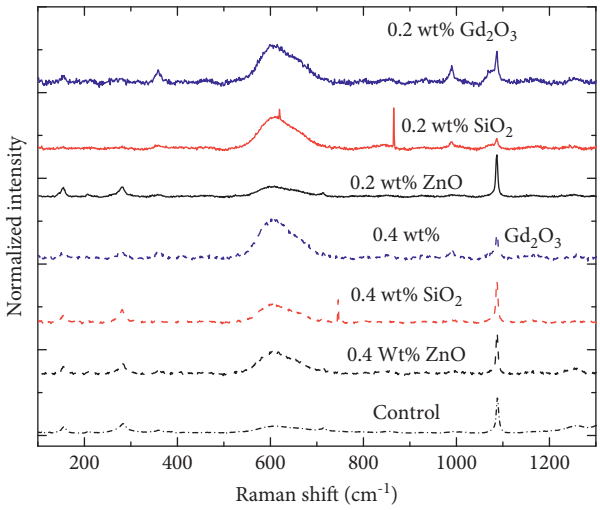

Figure 5: Raman spectra for cement paste matrices with 0.2 wt% ZnO, SiO_2, Gd_2O_3 (solid lines) and 0.4 wt% ZnO, SiO_2, Gd_2O_3 (dashed line) vs. the control samples (dash dot lines).

whereas specimens prepared with 0.2 wt% of SiO_2 do not show these features very clearly. In addition, the cement paste specimens with 0.4 wt% of SiO_2 show a relatively weaker CSH band at 605 cm^{-1} whereas, in the 0.2 wt% specimens, this is the strongest. The same band is unchanged in its intensity in the Gd_2O_3-cement matrix in both the samples prepared with 0.2 wt% and 0.4 wt% with the difference that the latter shows bands with narrower peak width. The CSH band at 605 cm^{-1} is stronger in all the specimens prepared with oxide additives when compared with control and CNT-cement paste matrices. It clearly manifests that the oxide additives have a dramatic effect on the hydration chemical process.

3.3. Reaction Kinetics. Tricalcium silicate (C3S) is a major composite mineral in the ordinary Portland cement. A generally written chemical equation (equation 1) for hydration process of C3S is,

$$3CaO \cdot SiO_2 + 2H_2O \longrightarrow 2CaO \cdot SiO_2 \cdot H_2O + CaH_2O_2. \quad (1)$$

However, it is expected that in presence of oxide additives, the chemical reaction will be modified. The reaction of C_3S with with ZnO and water would form CSH, calcium hydroxide (CaH_2O_2) and zinc hydroxide (ZnH_2O_2) as described in the chemical equation (2).

$$3CaO \cdot SiO_2 + 3H_2O + ZnO \longrightarrow 2CaO \cdot SiO_2 \cdot H_2O + CaH_2O_2 + ZnH_2O_2. \quad (2)$$

The additional band observed at 207 cm^{-1} in the ZnO-OPC matrix is contributed by zinc hydroxide (ZnH_2O_2). Similarly, C_3S reacts with the gadolinium oxide (Gd_2O_3) and water to make CSH, CaH_2O_2 and gadolinium hydroxide (GdH_3O_3) as shown in the chemical equation (3).

$$3CaO \cdot SiO_2 + 5H_2O + Gd_2O_3 \longrightarrow 2CaO \cdot SiO_2 \cdot H_2O + CaH_2O_2 + 2GdH_3O_3. \quad (3)$$

A distinguished Raman band from GdH_3O_3 is observed at 211 cm^{-1} in the Raman spectrum of Gd_2O_3 cement paste matrix.

The chemical equations 1–3 clearly show that more water molecules participate in the reaction when zinc oxide and gadolinium oxide are present in the cement paste. While, there are 2 water molecules participating in the chemical reaction (equation 3), in presence of ZnO there are 3 water molecules (equation 1) and in presence of Gd_2O_3, there are 5 water molecules (equation 2) taking part in the hydration. This is the origin of the strong Raman bands are observed at 605 cm^{-1} in the matrices containing the zinc and gadolinium oxide additives.

Furthermore, a strong CSH Raman band at 605 cm^{-1} is observed only for the ZnO 0.4 wt% cement paste. However, when compared to Gd_2O_3 cement paste matrix, the CSH band at 605 cm^{-1} is the strongest for both 0.2 wt% and 0.4 wt% specimens. It is well known that tri- and dicalcium silicates are not in their purest form in OPC. Instead, their chemical formulae in the ordinary Portland cement are reported [25] to be $Ca_{3.09}Si_{0.63}Fe_{0.22}A_{0.14}Mg_{0.06}S_{0.05}Ti_{0.01}K_{0.01}Cr_{0.01}$ for tricalcium silicate and $Ca_{2.48}Si_{0.51}Fe_{0.18}Al_{0.11}Mg_{0.05}S_{0.04}Ti_{0.01}K_{0.01}$ for dicalcium silicate. So, the Ca/Si ratio is greater than 5 in the specimens indicating that the tobermorite and jennite are far from being perfect crystals and there are Si vacancies. The Zn and Gd atoms contributed by the oxides occupy the Si vacancies and thus significantly modify the crystal structure of tobermorite and jennite. Moreover, the spectra of Gd_2O_3 matrices also show that the calcium carbonate peaks have become weak at around 1080 cm^{-1} which is not the case with matrices prepared with ZnO. The Gd^{3+} is a rare Earth metal and has a propensity to oxidize [31, 32] very quickly, not leaving enough oxygen atoms to form carbonates in the Gd_2O_3 matrix with OPC. On the other hand, the SiO_2 matrix shows interesting behavior. While the CSH products are high in concentration for the 0.2 wt% of SiO_2 in the cement paste, it decreases quite significantly when concentration of SiO_2 is increased upto 0.4 wt%. This observation is in agreement with a previous study [33] which showed that with the increasing SiO_2 in the cement paste, the space between the CSH domains increases which creates pores and voids thus reducing the compressive strength of the specimen.

4. Conclusion

The concentration of the CSH in the cement matrix with CNTs, ZnO, Gd_2O_3, and SiO_2 is compared by Raman spectroscopy. The major outcome of this study is as follows:

(i) The CNTs do not react chemically and therefore, CSH concentration is unchanged in the resultant matrices when compared to the control.

(ii) Metal oxides actively participate in the hydration process and form new hydrates such as ZnH_2O_2 and GdH_3O_3. The oxide additives, thus, have profound effects on the CSH concentration in the matrix.

(iii) The Raman spectrum of the ZnO-OPC matrix shows a strong CSH vibrational band indicating that the concentration of CSH increases with the increase of the ZnO weight percentage in the matrix.

(iv) Similarly, a strong CSH band is observed in the Gd_2O_3 cement matrix as well. However, the $CaCO_3$ band has become significantly weak in the Gd_2O_3 cement matrix. This indicates that the Gd^{3+}, with their strong ability to form oxides and hydrides, have bonded with the CO_2 in the atmosphere.

(v) Finally, for SiO_2 cement paste matrix, CSH concentration weakens when the weight percentage of the SiO_2 is increased, in agreement with the previous studies where decreasing Ca/Si also caused the compressive strength to decrease as well [33].

Data Availability

The data used to support the findings of this study are available from the author upon request.

Disclosure

The preprint of the manuscript is available at researchsquare.com [28].

Conflicts of Interest

The authors declare that they have no conflicts of interest.

Acknowledgments

The preprint of the manuscript is available at researchsquare.com [28]. The authors would like to acknowledge the support provided by the University of Sharjah competitive research grant 1802143076 and the Advance Materials Labs. The authors would also like to acknowledge Dr. Hussain Alawadhi for his help during the lab testing.

References

[1] F. Liu, Z. Sun, and C. Qi, "Raman spectroscopy study on the hydration behaviors of Portland cement pastes during setting," *Journal of Materials in Civil Engineering*, vol. 27, Article ID 04014223, 2014.

[2] W. Li, X. Li, S. J. Chen, G. Long, Y. M. Liu, and W. H. Duan, "Effects of nanoalumina and graphene oxide on early-age hydration and mechanical properties of cement paste," *Journal of Materials in Civil Engineering*, vol. 29, no. 9, Article ID 04017087, 2017.

[3] V. Stroganov, E. Sagadeev, R. Ibragimov, and L. Potapova, "Mechanical activation effect on the biostability of modified cement compositions," *Construction and Building Materials*, vol. 246, Article ID 118506, 2020.

[4] M. Tarrida, M. Madon, B. Le Rolland, and P. Colombet, "An in-situ Raman spectroscopy study of the hydration of tricalcium silicate," *Advanced Cement Based Materials*, vol. 2, no. 1, pp. 15–20, 1995.

[5] F. Liu and Z. Sun, "Chemical mapping of cement pastes by using confocal Raman spectroscopy," *Frontiers of Structural and Civil Engineering*, vol. 10, no. 2, pp. 168–173, 2016.

[6] B. Lothenbach, G. Le Saout, E. Gallucci, and K. Scrivener, "Influence of limestone on the hydration of Portland

cements," *Cement and Concrete Research*, vol. 38, no. 6, pp. 848–860, 2008.

[7] S. S. Kutanaei, D. Ph, and A. J. Choobbasti, "Effects of nanosilica particles and randomly distributed fibers on the ultrasonic pulse velocity and mechanical properties of cemented," *Sand*, vol. 29, pp. 1–9, 2017.

[8] A. Carriço, J. A. Bogas, A. Hawreen, and M. Guedes, "Durability of multi-walled carbon nanotube reinforced concrete," *Construction and Building Materials*, vol. 164, pp. 121–133, 2018.

[9] A. Tamimi, N. M. Hassan, K. Fattah, and A. Talachi, "Performance of cementitious materials produced by incorporating surface treated multiwall carbon nanotubes and silica fume," *Construction and Building Materials*, vol. 114, pp. 934–945, 2016.

[10] S. K. Adhikary, Ž. Rudžionis, and R. Rajapriya, "The effect of carbon nanotubes on the flowability, mechanical, microstructural and durability properties of cementitious composite: an overview," *Sustainability*, vol. 12, no. 20, pp. 1–25, 2020.

[11] M. Azeem and M. Azhar Saleem, "Role of electrostatic potential energy in carbon nanotube augmented cement paste matrix," *Construction and Building Materials*, vol. 239, Article ID 117875, 2020.

[12] S. Lv, Y. Ma, C. Qiu, T. Sun, J. Liu, and Q. Zhou, "Effect of graphene oxide nanosheets of microstructure and mechanical properties of cement composites," *Construction and Building Materials*, vol. 49, pp. 121–127, 2013.

[13] A. Mohammed, J. G. Sanjayan, W. H. Duan, and A. Nazari, "Incorporating graphene oxide in cement composites: a study of transport properties," *Construction and Building Materials*, vol. 84, pp. 341–347, 2015.

[14] Z. Zhao, T. Qi, W. Zhou et al., "A review on the properties, reinforcing effects, and commercialization of nanomaterials for cement-based materials," *Nanotechnology Reviews*, vol. 9, no. 1, pp. 303–322, 2020.

[15] N. M. Hassan, K. P. Fattah, and A. K. Tamimi, "Modelling mechanical behavior of cementitious material incorporating CNTs using design of experiments," *Construction and Building Materials*, vol. 154, pp. 763–770, 2017.

[16] K. Gong, S. M. Asce, Z. Pan et al., "Reinforcing effects of graphene oxide on," *Portland Cement Paste*, vol. 27, pp. 1–6, 2015.

[17] F. U. A. Shaikh, S. W. M. Supit, and S. Barbhuiya, "Microstructure and nanoscaled characterization of HVFA cement paste containing nano—SiO_2 and Nano—$CaCO_3$," *Journal of Materials in Civil Engineering*, vol. 29, pp. 1–10, 2017.

[18] J. Han, Y. Liang, W. Sun, W. Liu, and S. Wang, "Microstructure modification of carbonated cement paste with six kinds of modern," *Microscopic Instruments*, vol. 27, pp. 1–14, 2015.

[19] M. A. Kafi, A. Sadeghi-nik, A. Bahari, A. Sadeghi-nik, and E. Mirshafiei, "Microstructural characterization and mechanical properties of cementitious mortar containing montmorillonite nanoparticles," *Journal of Materials in Civil Engineering*, vol. 28, pp. 1–10, 2016.

[20] F. U. A. Shaikh and S. W. M. Supit, "Effects of superplasticizer types and mixing methods of nanoparticles on compressive strengths of cement," *Pastes*, vol. 28, pp. 1–7, 2016.

[21] W. Han, T. Sun, X. Li, M. Sun, and Y. Lu, "Using of borosilicate glass waste as a cement additive," *Nuclear Instruments and Methods in Physics Research Section B: Beam Interactions with Materials and Atoms*, vol. 381, pp. 11–15, 2016.

[22] Z. Lu, C. Lu, C. K. Y. Leung, and Z. Li, "Graphene oxide modified strain hardening cementitious composites with enhanced mechanical and thermal properties by incorporating ultra-fine phase change materials," *Cement and Concrete Composites*, vol. 98, pp. 83–94, 2019.

[23] Y. Tao, W. Zhang, D. Shang et al., "Comprehending the occupying preference of manganese substitution in crystalline cement clinker phases: a theoretical study," *Cement and Concrete Research*, vol. 109, pp. 19–29, 2018.

[24] L. Chi, A. Zhang, Z. Qiu et al., "Hydration activity, crystal structural, and electronic properties studies of Ba-doped dicalcium silicate," *Nanotechnology Reviews*, vol. 9, no. 1, pp. 1027–1033, 2020.

[25] M. Azeem and M. Azhar Saleem, "Hydration model for the OPC-CNT mixture: theory and experiment," *Construction and Building Materials*, vol. 264, Article ID 120691, 2020.

[26] M. Azeem, M. T. Junaid, and M. A. Saleem, "Correlated strength enhancement mechanisms in carbon nanotube based geopolymer and OPC binders," *Construction and Building Materials*, vol. 305, Article ID 124748, 2021.

[27] D. Lu, X. Shi, J. Zhong, D. Lu, X. Shi, and J. Zhong, "Understanding the role of unzipped carbon nanotubes in cement pastes," *Cement and Concrete Composites*, vol. 126, Article ID 104366, 2022.

[28] M. Azeem, https://assets.researchsquare.com/files/rs-895716/v1/54236e93-0765-4b92-bff7-04f9bad8db67.pdf?c=1631896020.

[29] X. Zhao, Y. Ando, L.-C. Qin, H. Kataura, Y. Maniwa, and R. Saito, "Multiple splitting of G-band modes from individual multiwalled carbon nanotubes," *Applied Physics Letters*, vol. 81, no. 14, pp. 2550–2552, 2002.

[30] S.-L. Zhand, *Raman Spectroscopy and its Application N Nanostructures*, John Wiley & Sons, Hoboken, NJ, USA, 2012.

[31] M. Azeem, "Spin-split joint density of states in GdN," *Chinese Physics Letters*, vol. 33, no. 2, Article ID 027501, 2016.

[32] M. Azeem, "Spin polarized conduction and valence band states in GdN," *MRS Advances*, vol. 2, no. 3, pp. 153–158, 2017.

[33] W. Kunther, S. Ferreiro, and J. Skibsted, "Influence of the Ca/Si ratio on the compressive strength of cementitious calcium-silicate-hydrate binders," *Journal of Materials Chemistry*, vol. 5, no. 33, pp. 17401–17412, 2017.